Acta Crystallographica Section D
Biological Crystallography
ISSN 0907-4449

Structures of *Arthrobacter globiformis* urate oxidase–ligand complexes

Ella Czarina Magat Juan,[a]‡ Md Mominul Hoque,[a] Satoru Shimizu,[a] Md Tofazzal Hossain,[a]§ Tamotsu Yamamoto,[b] Shigeyuki Imamura,[b] Kaoru Suzuki,[c] Masaru Tsunoda,[d] Hitoshi Amano,[e] Takeshi Sekiguchi[c] and Akio Takénaka[a,e]*

[a]Graduate School of Bioscience and Biotechnology, Tokyo Institute of Technology, 4259 Nagatsuta, Midori-ku, Yokohama, Kanagawa 226-8501, Japan, [b]Asahi Kasei Pharma Corporation, Mifu-ku, Izunokuni-shi, Shizuoka 410-2321, Japan, [c]Fukushima National College of Technology, Taira-kamiarakawa, Iwaki 970-8034, Japan, [d]College of Science and Engineering, Iwaki Meisei University, Chuodai-iino, Iwaki 970-8551, Japan, and [e]Faculty of Pharmacy, Iwaki Meisei University, Chuodai-iino, Iwaki 970-8551, Japan

‡ Present address: Graduate School of Science, The University of Tokyo, Japan.
§ Present address: Department of Biochemistry and Molecular Biology, University of Rajshahi, Bangladesh.

Correspondence e-mail: atakenak@bio.titech.ac.jp

Received 19 February 2008
Accepted 7 May 2008

PDB References: *Ag*UOX, complex with uric acid, 2yzb, r2yzbsf; complex with allantoate, 2yzc, r2yzcsf; complex with 9-azaxanthin, 2yzd, r2yzdsf; native, 2yze, r2yzesf.

The enzyme urate oxidase catalyzes the conversion of uric acid to 5-hydroxyisourate, one of the steps in the ureide pathway. *Arthrobacter globiformis* urate oxidase (*Ag*UOX) was crystallized and structures of crystals soaked in the substrate uric acid, the inhibitor 8-azaxanthin and allantoin have been determined at 1.9–2.2 Å resolution. The biological unit is a homotetramer and two homotetramers comprise the asymmetric crystallographic unit. Each subunit contains two T-fold domains of $\beta\beta\alpha\alpha\beta\beta$ topology, which are usually found in purine- and pterin-binding enzymes. The uric acid substrate is bound tightly to the enzyme by interactions with Arg180, Leu222 and Gln223 from one subunit and with Thr67 and Asp68 of the neighbouring subunit in the tetramer. In the other crystal structures, lithium borate, 8-azaxanthin and allantoate are bound to the enzyme in a similar manner as uric acid. Based on these *Ag*UOX structures, the enzymatic reaction mechanism of UOX has been proposed.

1. Introduction

Urate oxidase (uricase or UOX; EC 1.7.3.3), an enzyme present in various species, catalyzes the oxidation of uric acid, resulting in the formation of ureides (Fig. 1*a*). UOX is beneficial to some bacteria, which thrive on uric acid as their sole source of carbon and nitrogen. In leguminous plants, UOX is a crucial enzyme in the nitrogen-assimilation pathway. In addition, a number of mammals utilize UOX to dispose of excess nitrogen. However, higher primates, including humans, lack a functional UOX as a consequence of mutations and deletions within the coding sequence of the gene (Wu *et al.*, 1992). This is believed to confer a selective advantage because uric acid may prevent the occurrence of cancer (Ames *et al.*, 1981; Sevenian *et al.*, 1991). On the other hand, elevated serum uric acid levels can lead to gouty arthritis and renal stones (Cameron & Simmonds, 1981; Terkeltaub, 1993). Thus, UOX is used as a drug for the treatment of tophaceous gout (Rozenberg *et al.*, 1995) and for the prevention and treatment of hyperuricaemia associated with lymphoid malignancies (Pui *et al.*, 1997).

Initially, uric acid was thought to be converted to allantoin in a single step catalyzed by UOX. Recent studies, however, have shown that two further ureides, 5-hydroxyisourate and 2-oxo-4-hydroxy-4-carboxy-5-ureidoimidazoline, are formed prior to allantoin and that their formation is catalyzed by two other enzymes (Fig. 1*a*; Kahn & Tipton, 1997, 1998; Sarma *et al.*, 1999; Raychaudhuri & Tipton, 2002). Allantoin undergoes a further series of degradation steps, again catalyzed by different enzymes, to generate allantoate, ureidoglycolate, glyoxylate and urea. UOX is unique among the oxygen-requiring enzymes in the sense that it does not need a cofactor

to convert uric acid to 5-hydroxyisourate. It has been reported that O_2 is reduced to H_2O_2 and that a solvent molecule provides the O atom that is attached to C5 in 5-hydroxyisourate (Bentley & Neuberger, 1952; Kahn & Tipton, 1997; Kahn *et al.*, 1997).

Here, we present the structures of *Arthrobacter globiformis* UOX (*Ag*UOX) crystals soaked in several ligands: the substrate uric acid, allantoin and the inhibitor 8-azaxanthin (Fig. 1*b*). Although several crystal structures of UOX from *A. flavus* (*Af*UOX) are available (Colloc'h *et al.*, 1997, 2006, 2008; Retailleau *et al.*, 2004, 2005; Gabison *et al.*, 2006), this is the first report of the structure of UOX with the uric acid subtrate (or intermediate) and with the product allantoate. The structures also provide several interesting structural details that have not previously been observed in the structure of *Af*UOX.

2. Materials and methods

2.1. Enzyme expression and purification

A plasmid containing the *Ag*UOX gene was introduced into the expression host cell *Escherichia coli* DH1. Cells were grown for 20 h at 310 K in BHI medium and were collected by centrifugation at 7000*g* for 10 min. Pellets were suspended in 10 m*M* phosphate buffer pH 7.0 containing 0.2% lysozyme. The cell suspension was incubated at 310 K for 2 h with continuous stirring. The supernatant obtained by centrifugation at 7000*g* for 20 min was loaded onto a DEAE-Sepharose FF column. The enzyme was eluted with a linear gradient of 0.1–0.3 *M* KCl in 10 m*M* phosphate buffer pH 7.0. Ammonium sulfate (13%) was added to the pooled enzyme fractions. The fractions were applied onto a Phenyl-Sepharose column and the enzyme was eluted with a linear gradient of 13–5% ammonium sulfate in 10 m*M* phosphate buffer pH 7.0. The fractions containing the enzyme were combined and concentrated by membrane filtration (Microcon YM3).

2.2. Crystallization

Lyophilized *Ag*UOX was dissolved in 50 m*M* sodium borate buffer pH 9.0 to a concentration of 10 mg ml^{-1}. Crystallizations were performed using the hanging-drop vapour-diffusion method at 293 K. The enzyme was crystallized in droplets consisting of equal volumes (2.5 µl) of enzyme solution and reservoir solution, which contained 0.5 *M* lithium sulfate, 8.5%(*w*/*v*) PEG 8000 and 50 m*M* sodium borate buffer pH 9.0. The crystals were placed for 20 h in soaking solutions containing 8-azaxanthin, uric acid or allantoin, each of which was dissolved in the reservoir solution to a concentration of 5 mg ml^{-1}.

2.3. X-ray data collection and data processing

The X-ray diffraction measurements were performed at 100 K. For the native (*Ag*UOX-native), 8-azaxanthin-soaked (*Ag*UOX-AZA) and allantoin-soaked (*Ag*UOX-ALN) crystals, diffraction data were collected on the NW12 beamline of the Photon Factory (Ibaraki, Japan) using an ADSC Quantum 210 CCD detector (λ = 1.00 Å). For the crystal soaked in uric acid (*Ag*UOX-UA), diffraction data were collected using an ADSC Quantum 315 CCD detector on the BL5A beamline of the Photon Factory (λ = 1.00 Å). The data for the *Ag*UOX-native crystal were processed with *CrystalClear* (Pflugrath, 1999), while those for the *Ag*UOX-AZA, *Ag*UOX-ALN and *Ag*UOX-UA crystals were processed with *HKL*-2000 (Otwinowski & Minor, 1997). Statistics of data collection and crystal data are given in Table 1.

2.4. Structure determination and refinement

The *Ag*UOX-native structure was solved by molecular replacement using the program *AMoRe* (Navaza, 1994) with a tetramer of UOX from *A. flavus* (PDB code 1r51) generated from the monomeric structure as a search model. The atomic

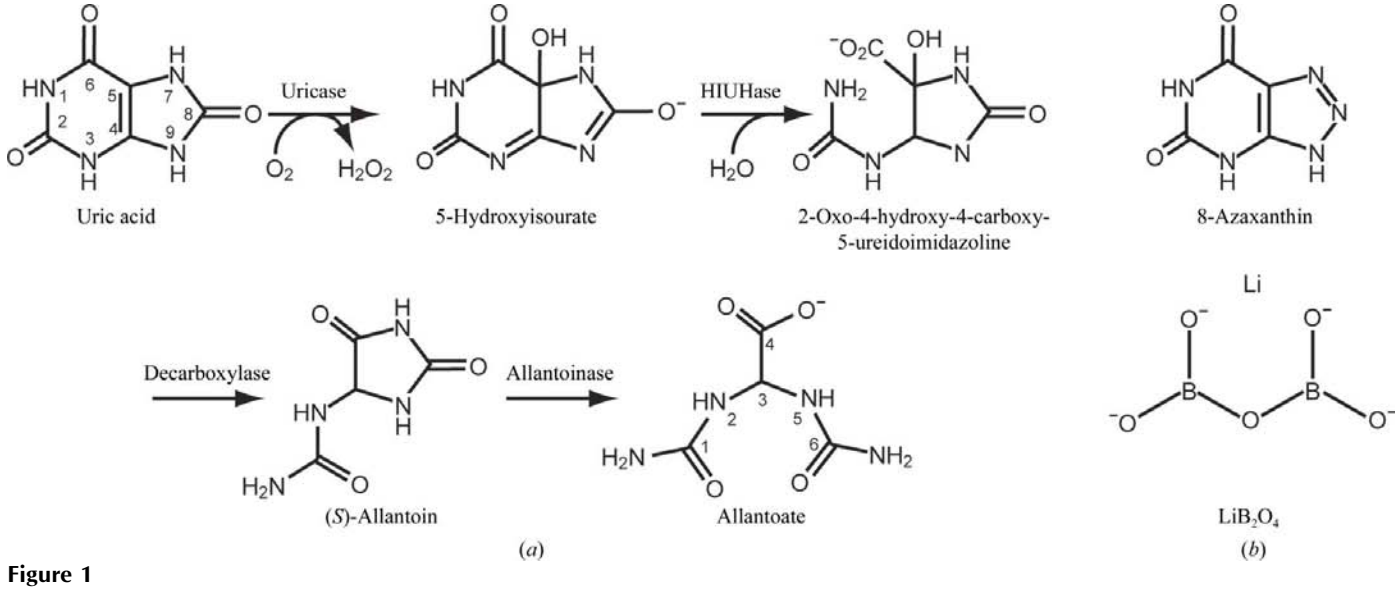

Figure 1
(*a*) Schematic representation of the ureide pathway responsible for the oxidation of uric acid to allantoate (Kahn & Tipton, 1998). (*b*) The chemical structures of 8-azaxanthin and lithium borate.

Table 1
Statistics of data collection and crystal data.

Values in parentheses are for the highest resolution shell.

	*Ag*UOX-UA	*Ag*UOX-ALN	*Ag*UOX-AZA	*Ag*UOX-native
Data collection				
X-ray source	Photon Factory			
Beamline	BL5A	NW12	NW12	NW12
Wavelength (Å)	1.00	1.00	1.00	1.00
Exposure time per frame (s)	5	10	5	8
Angular increment per frame (°)	0.3	0.5	0.5	0.2
Total rotation range (°)	180	180	180	180
Crystal-to-detector distance (mm)	250	270	220	190
Crystal data				
Space group	$P2_12_12_1$	$P2_12_12_1$	$P2_12_12_1$	$P2_12_12_1$
Unit-cell parameters				
a (Å)	84.5	85.5	83.3	85.4
b (Å)	123.2	122.9	122.3	122.5
c (Å)	284.6	284.8	283.9	284.5
Z′†	8	8	8	8
Data reduction				
Software	*HKL*-2000	*HKL*-2000	*HKL*-2000	*CrystalClear*
Resolution range (Å)	50.0–1.90 (1.97–1.90)	50.0–1.88 (1.95–1.88)	20.0–2.24 (2.32–2.24)	42.2–1.99 (2.06–1.99)
No. of observed reflections	1244917	1421740	739628	1260560
No. of unique reflections	213158	231814	132537	193433
Completeness (%)	90.9 (73.5)	95.2 (83.9)	97.4 (87.7)	91.8 (87.1)
$R_{\rm merge}$‡ (%)	0.090 (0.341)	0.074 (0.269)	0.067 (0.237)	0.060 (0.177)
$I/\sigma(I)$	4.0 (8.6)	1.8 (5.3)	3.1 (7.7)	4.7 (12.3)
Redundancy	5.8 (5.7)	6.1 (5.7)	5.4 (5.4)	3.5 (3.3)

† Number of subunits in the asymmetric unit. ‡ $R_{\rm merge} = \sum_{hkl}\sum_i |I_i(hkl) - \langle I(hkl)\rangle|/\sum_{hkl}\sum_i I_i(hkl)$, where $I_i(hkl)$ is the *i*th measurement of the intensity of reflection *hkl* and $\langle I(hkl)\rangle$ is its mean value.

Table 2
Statistics of structure refinement.

	*Ag*UOX-UA	*Ag*UOX-ALN	*Ag*UOX-AZA	*Ag*UOX-native
Resolution range (Å)	20.0–1.90	20.0–1.90	20.0–2.24	10.0–1.99
No. of reflections used ($F_o > 3\sigma$)	184396	212385	118368	190430
R factor† (%)	19.0	18.0	18.9	19.1
$R_{\rm free}$‡ (%)	22.3	20.9	23.9	21.8
R.m.s. deviation				
Bond lengths (Å)	0.005	0.005	0.006	0.007
Bond angles (°)	1.3	1.3	1.3	1.4
No. of protein atoms	18284	18256	18284	18256
No. of ligand atoms				
Lithium borate	—	—	—	56
8-Azaxanthin	—	—	96	—
Uric acid	96	—	—	—
Allantoate	—	96	—	—
No. of waters	1360	1990	1160	1836
Ramachandran plot: residues in (%)				
Most favoured regions	89.7	90.3	89.4	91.2
Allowed regions	10.3	9.7	10.6	8.8

† *R* factor = $100 \times \sum ||F_o| - |F_c||/\sum |F_o|$, where $|F_o|$ and $|F_c|$ are the observed and calculated structure-factor amplitudes, respectively. ‡ Calculated using a random set containing 10% of observations that were not included throughout refinement (Brünger, 1992).

parameters were initially refined by the rigid-body and restrained maximum-likelihood least-squares techniques in *REFMAC*5 from the *CCP*4 suite (French & Wilson, 1978; Collaborative Computational Project, Number 4, 1994). Strict noncrystallographic symmetry was used to constrain the subunits to be identical during the early stages of refinement, but was later relaxed to allow independent refinement of the subunits. The structure was revised by interpreting OMIT maps at every residue. After several rounds of refinement with *REFMAC*5, crystallographic conjugate-gradient minimization and *B*-factor refinements were performed with the program *CNS* (Brünger *et al.*, 1998). The *Ag*UOX-AZA, *Ag*UOX-ALN and *Ag*UOX-UA structures were also solved by molecular replacement using *AMoRe* with the refined *Ag*UOX-native structure as the initial model. Refinements were performed in the same manner as described above with the programs *REFMAC*5 and *CNS*.

Statistics of refinement for all the *Ag*UOX structures are summarized in Table 2. The OMIT maps of the ligands drawn with the program *O* (Jones *et al.*, 1991) are shown in Fig. 2. Fig. 3 was drawn with *PyMOL* (DeLano Scientific; http://www.pymol.org) and Fig. 4 with *RASMOL* (Sayle & Milner-White, 1995). The final structures were validated using *PROCHECK* (Laskowski *et al.*, 1993) and *MOLPROBITY* (Lovell *et al.*, 2003). Sequence alignments were performed with *ClustalX* (Chenna *et al.*, 2003). Structural comparisons were carried out using *Swiss-PdbViewer* (http://www.expasy.org/spdbv/). Protein interfaces were measured using the Protein–Protein Interaction Server (http://www.biochem.ucl.ac.uk/bsm/PP/server/).

3. Results and discussion

3.1. Structure determination and quality

The *Ag*UOX structures were determined at resolutions ranging from 1.9 to 2.2 Å with *R* and $R_{\rm free}$ values below 19% and 24%, respectively. The asymmetric units of all the *Ag*UOX crystals contain two tetramers, each composed of four identical subunits. The large number of subunits in the asymmetric unit is somewhat unexpected, but calculation of the Matthews coefficients (V_M; Matthews, 1968) and comparison of the crystal environments suggested that there were eight subunits in the asymmetric unit. One subunit consists of 287 amino-acid residues. Residues 1–10 in the N-terminus and residues 298–302 in the C-terminus are not clearly visible in the electron density and were excluded from refinement. In *Ag*UOX-native and *Ag*UOX-ALN, the side chains of Lys12 and of Asp291 were disordered and were not included in the final structures. The eight subunits in each structure superimposed well within a root-mean-square (r.m.s.) deviation of 0.36 Å for the C^α

atoms. All nonglycine residues are within the most favoured and allowed regions of Ramachandran plots (Ramachandran *et al.*, 1963).

One molecule of lithium borate, which is a component of the crystallization mother liquor, was introduced into each subunit of the *Ag*UOX-native structure. Similarly, eight molecules of 8-azaxanthin and uric acid (one per subunit) were added to the *Ag*UOX-AZA and *Ag*UOX-UA structures, respectively. However, $|F_o| - |F_c|$ maps of *Ag*UOX-ALN suggested that the bound molecules were allantoate and not allantoin (Fig. 2). Despite the different ligands, comparisons of the four *Ag*UOX structures yielded r.m.s. deviations of below 0.32 Å, suggesting that the ligands have similar structural effects.

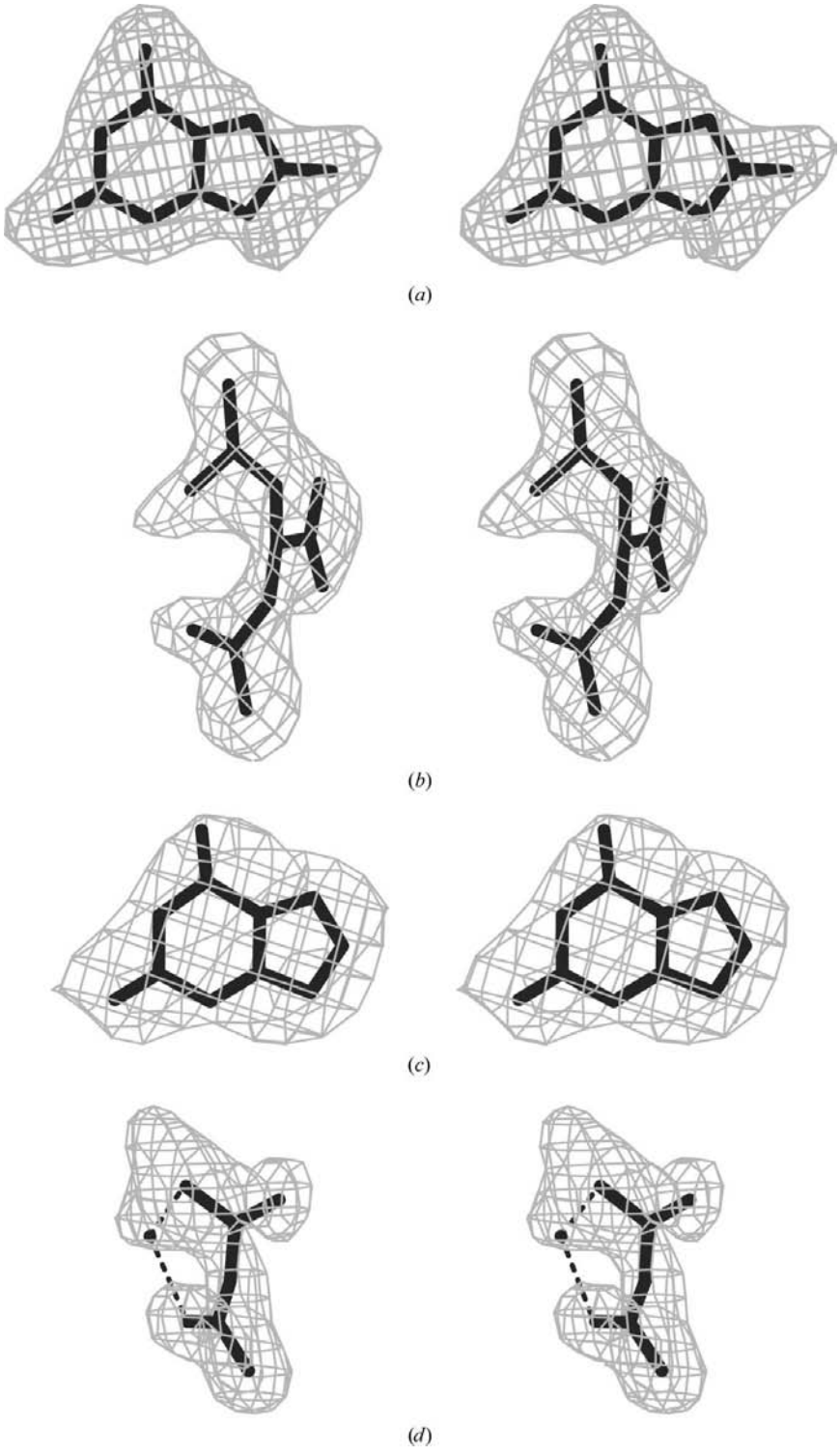

Figure 2
Stereoviews of OMIT maps contoured at the 2σ level for (*a*) uric acid, (*b*) allantoate, (*c*) 8-azaxanthin and (*d*) lithium borate bound in the *Ag*UOX-UA, *Ag*UOX-ALN, *Ag*UOX-AZA and *Ag*UOX-native structures, respectively.

3.2. Overall structure of *Ag*UOX and comparison with *Af*UOX structures

The structure of the *Ag*UOX monomer and the secondary-structure elements are shown in Fig. 3(*a*). Each monomer contains eight long β-strands (S1–S8), three short β-strands (s3′, s7′ and s8′), four α-helices (H1–H4) and two one-turn helices (h1 and h2). The monomer can be divided into two structurally similar domains known as T-fold domains (Colloc'h *et al.*, 1997), each with an antiparallel superfold $\beta\beta\alpha\alpha\beta\beta$ topology. The β-strands form a curved β-sheet and the α-helices are positioned on the concave side of the sheet. Comparisons of the structures of *Ag*UOX and *Af*UOX (Colloc'h *et al.*, 1997, 2006; Retailleau *et al.*, 2004, 2005; Gabison *et al.*, 2006) reveal that despite the deletions and extensions at the termini, the topology of the *Ag*UOX monomer is similar to that of *Af*UOX. The only differences are the absence of the one-turn helix between S6 and H3 (designated h2 in *Af*UOX) and of one short β-strand between S3 and S4 (designated s4′ in *Af*UOX) in *Ag*UOX and in the lengths of the β-strands and α-helices. Moreover, superposition of a tetramer of *Ag*UOX on that of *Af*UOX resulted in small r.m.s. deviations of up to 1.13 Å for 1048 C^{α} atoms.

Pairs of monomers (*A* and *D*, *B* and *C*, *A*′ and *D*′, and *B*′ and *C*′) are related by approximate twofold symmetry and are tightly bound to each other (Fig. 3*b*). The accessible surface area buried in the dimeric interface is about 3100 $Å^2$, which accounts for ∼20% of the whole accessible surface area. The dimeric interface includes up to 40 hydrogen bonds and extensive van der Waals interactions, primarily involving residues in the N-terminal ends of S1 of one subunit and S8 of an adjacent subunit.

Pairs of dimers (*A* + *D* and *B* + *C*, and *A*′ + *D*′ and *B*′ + *C*′) are stacked face-to-face to form a tetramer (Fig. 3*c*), which is the

functional unit of *Ag*UOX. The tetramer has overall dimensions of approximately 74 × 86 × 76 Å. A tunnel roughly 30 Å in diameter and 80 Å in length passes through the centre of the tetramer. Only about 2300 Å^2 (15%) of the whole accessible surface area is buried in the dimer–dimer interface. The interactions between two dimers include 39 hydrogen bonds and three salt bridges, most of which are formed by residues in S4 and S5.

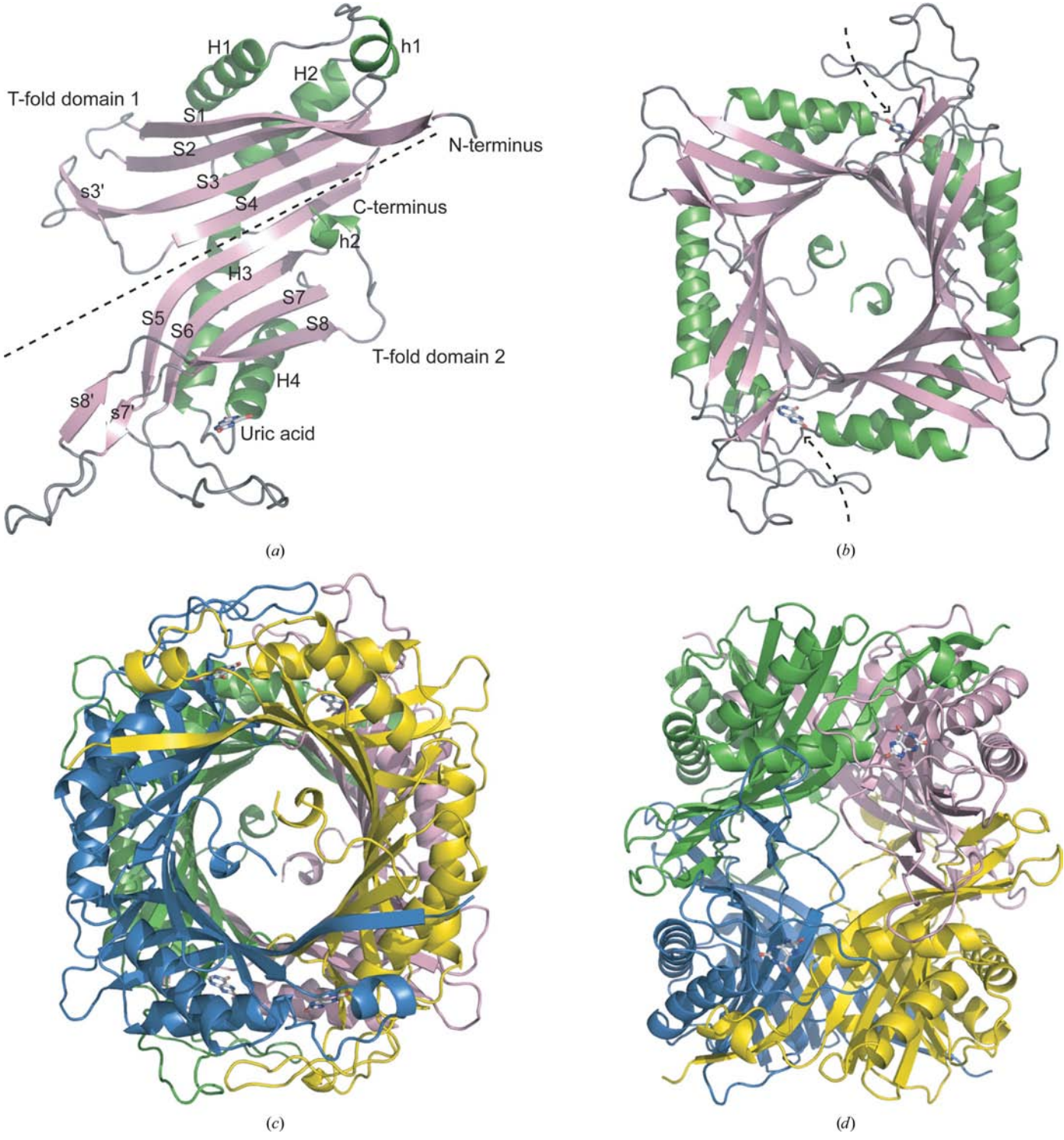

Figure 3
The overall structure of *Ag*UOX-UA. (*a*) The monomer of *Ag*UOX showing the two T-fold domains, the secondary-structural elements and the bound uric acid. S (or s) and H (or h) are used to indicate β-sheets and α-helices, respectively. (*b*) The dimer of *Ag*UOX showing the locations of the active sites. (*c*) and (*d*) Two orthogonal views of the tetramer of *Ag*UOX with subunits *A*, *B*, *C* and *D* coloured green, blue, yellow and pink, respectively. The uric acid molecules are shown as stick representations.

3.3. Active site

The active sites are located at the interfaces between *A* and *D*, *B* and *C*, *A*′ and *D*′, and *B*′ and *C*′ (Fig. 3*b*). One subunit contributes residues from the N-terminal region of H4 and the region from S6 to S8, while the other subunit contributes residues from S1 and the N-terminal region of H1 (residues from the neighbouring subunit are marked with an asterisk from here on). The active-site opening is formed by the coiled region between S5 and S6 and the region from s7′ to s8′. There are a total of eight active sites in the asymmetric unit, four per functional tetramer.

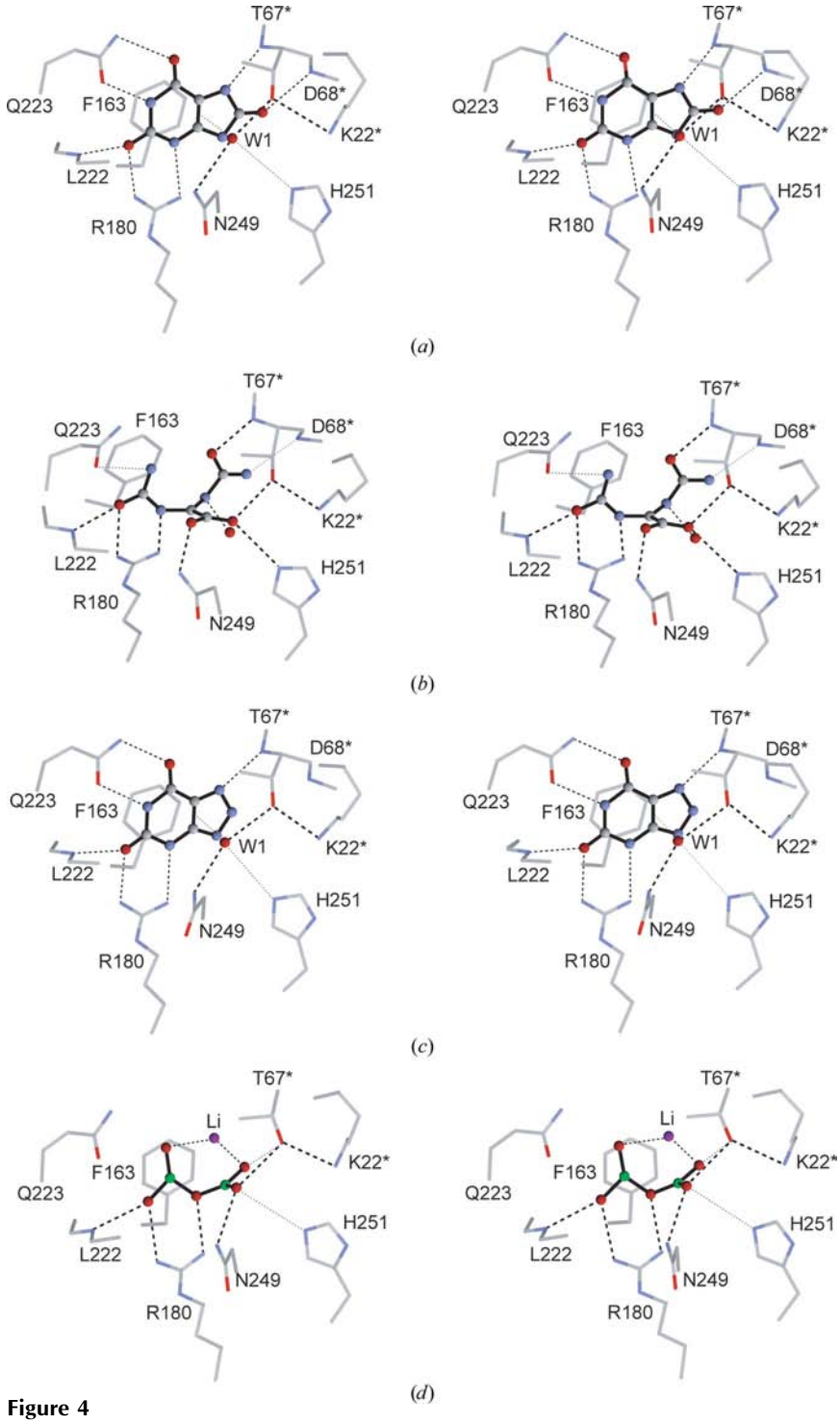

Figure 4
Stereoviews of the active sites in the *Ag*UOX structures showing the interactions of (*a*) uric acid, (*b*) allantoate, (*c*) 8-azaxanthin and (*d*) lithium borate with the enzyme. The ligands are shown as black ball-and-stick representations. The B and Li atoms are shown as green and purple spheres and the O atoms and water molecules are shown as red spheres. Residues marked with an asterisk belong to the neighbouring subunit. The dashed and dotted lines indicate possible hydrogen bonds and van der Waals interactions, respectively.

3.3.1. Ligand binding in the *Ag*UOX-UA structure. An $|F_o| - |F_c|$ electron-density map of the *Ag*UOX-UA crystal calculated in the absence of the soaked molecules suggested that the bound ligand in the active site could either be the substrate uric acid (Fig. 2*a*; refer to Fig. 1 for the numbering of the atoms) or a reaction intermediate whose atoms are positioned almost identically to those of uric acid. Further studies are required in order to elucidate the state of the trapped molecule. Nevertheless, the binding interactions in the present *Ag*UOX-UA structure could provide details essential for understanding uric acid catalysis, regardless of the state of the trapped ligand. For the purpose of simplicity, the ligand was assigned as uric acid.

As shown in Fig. 4(*a*), two residues that are strictly conserved throughout the urate oxidase family, Gln223 and Arg180, anchor the six-membered ring of uric acid to the enzyme. The side-chain OE1 and NE2 atoms of Gln223 interact with N1 and O6 of uric acid, respectively, whereas the side-chain NH1 and NH2 atoms of Arg180 donate their H atoms to form two hydrogen bonds to N3 and O2 of uric acid. The main-chain amide of Leu222, the residue immediately preceding Gln223, also interacts with O2 of uric acid. The N7 and N8 atoms in the five-membered ring of uric acid are hydrogen bonded to the main-chain amides of Thr67* and Asp68* of the neighbouring subunit. The W1 water molecule, located just above the C4–C5 bond, is held in place by the side chains of Thr67* and Asn249. His251 NE2 is positioned at a distance of 4 Å from the water molecule, suggesting that this amino-acid residue could possibly trap and activate an oxygen molecule which could take the place of the water molecule. In addition to the Thr67*–Asn249–His251 triad, the side chain of Lys22*, which is surrounded by hydrophobic residues on one side, points toward the active site. Its location suggests its participation in the catalysis of uric acid. Another conserved residue, Phe163, is stacked below the substrate and is posi-

tioned at a distance of ~3.6 Å from the midpoint of the C4–C5 bond.

3.3.2. Binding of other ligands. The interactions of allantoate, 8-azaxanthin and lithium borate with *Ag*UOX are shown in Figs. 4(*b*), 4(*c*) and 4(*d*), respectively. The interactions of allantoate with Thr67* and Asp68* resemble those of uric acid. The five-membered ring of 8-azaxanthin is unable to maintain such interactions, while its six-membered ring forms similar hydrogen bonds as uric acid to Leu222, Gln223 and Arg180, which is to be expected since the six-membered rings of the two ligands are the same. It is noteworthy that the two water molecules are conserved in all four structures and these waters bridge the ligands to Arg180.

3.4. Mechanistic implications

Trapping of uric acid (or of an intermediate with the same atomic positioning as uric acid) in the present *Ag*UOX-UA structure allowed us to identify important interactions in UOX and to propose a scheme for the conversion of uric acid to 5-hydroxyisourate (Fig. 5). The urate oxidase reaction first proceeds with uric acid interacting with O_2, generating intermediates similar to those encountered in flavin-dependent monooxygenases (Kahn & Tipton, 1997; Kahn *et al.*, 1997). Single-turnover stopped-flow spectroscopic studies of urate oxidase from *Glycine max* have provided evidence that several intermediates are bound to the enzyme during the course of the reaction (Kahn & Tipton, 1998). The first intermediate, the urate dianion, is highly reactive and is believed to be the intermediate that directly reacts with O_2. The nature of the urate dianion is controversial and NMR titration (Kahn *et al.*, 1997) and UV spectrophotometric studies (Pfleiderer, 1974) have shown that in the absence of urate oxidase the 3,9-dianion is the most stable of the possible dianion states. However, the distances between N3 of uric acid and Arg180 NH1 (3.1 Å) and between N7 of uric acid and the main-chain amide of Thr67* (2.6 Å) in the *Ag*UOX-UA structure (Fig. 4*a*) suggest that the natural substrate is in the 3,7-dianion state. Two donor groups, the amides of Thr67* and Asp68*, interact with the N7 and O8 atoms of uric acid, respectively, on which a negative charge could possibly be delocalized. This is in agreement with recent quantum-mechanical studies (Altarsha *et al.*, 2007) and with the proposal of Prangé and colleagues (Retailleau *et al.*, 2004; Colloc'h *et al.*, 2008).

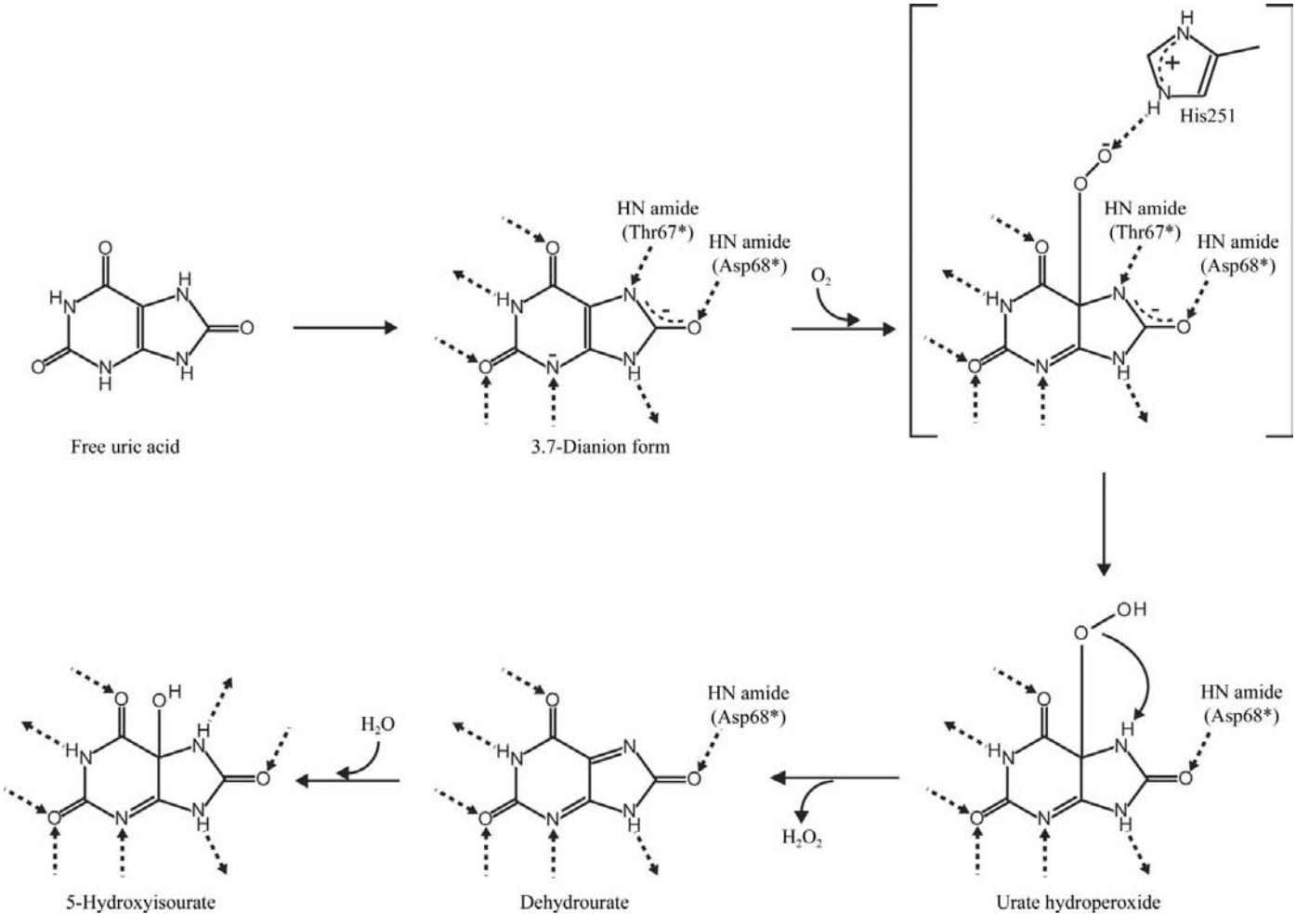

Figure 5
Proposed reaction mechanism for UOX.

The urate dianion would undergo oxidation, as demonstrated by model studies and computational methods (Kahn *et al.*, 1997), resulting in the formation of the second intermediate urate hydroperoxide. A dioxygen-bound model can reasonably be constructed by replacing the bound W1 O atom with one of the dioxygen atoms, so that the remaining O atom forms a hydrogen bond with His251 NE2. Therefore, His251 could be involved in the protonation of the dioxygen molecule. The locations of the two active-site residues in *Ag*UOX-UA, Thr67* and Lys22*, suggest their involvement in the proton transfer. The hydroxyl group of Thr67* binds to N7 of uric acid (distance = 2.9 Å) and to Lys22* NZ (distance = 3.0 Å). Lys22* NZ could also be hydrogen bonded to His251 NE2 (distance = 3.2 Å). Perfect conservation of these residues across the UOX family supports their possible functional role. Furthermore, the proposed mechanism is consistent with the results of site-directed mutagenesis of *Bacillus subtilis* UOX, in which K9M and T69A mutations (Lys9 and Thr69 in *B. subtilis* UOX correspond to Lys22 and Thr67 in *Ag*UOX, respectively) led to the loss of enzyme activity (Imhoff *et al.*, 2003).

Subsequent expulsion of H_2O_2 from urate hydroperoxide results in the generation of dehydrourate, the third putative intermediate, which has not yet been observed experimentally. It is worth noting that dehydrourate and the 3,7-dianion have nearly identical chemical structures. Hence, the trapped ligand in *Ag*UOX-UA could also be the dehyrourate intermediate. Dehydrourate is then hydrated to form the product 5-hydroxyisourate, most probably by the W1 water molecule which has been observed in all crystal structures of UOX.

We thank M. Suzuki, N. Igarashi and A. Nakagawa for help with data collection. This work was supported in part by Grants-in-Aid for the Protein 3000 Project for Metabolic Proteins (S. Kuramitsu) from the Ministry of Education, Culture, Sports, Science and Technology of Japan.

References

Altarsha, M., Monard, G. & Castro, B. (2007). *Int. J. Quantum Chem.* **107**, 172–181.
Ames, B. N., Cathcart, R., Schwiers, E. & Hochstein, P. (1981). *Proc. Natl Acad. Sci. USA*, **78**, 6858–6862.
Bentley, R. & Neuberger, A. (1952). *Biochem. J.* **52**, 694–699.
Brünger, A. T. (1992). *Nature (London)*, **355**, 472–475.
Brünger, A. T., Adams, P. D., Clore, G. M., DeLano, W. L., Gros, P., Grosse-Kunstleve, R. W., Jiang, J.-S., Kuszewski, J., Nilges, M., Pannu, N. S., Read, R. J., Rice, L. M., Simonson, T. & Warren, G. L. (1998). *Acta Cryst.* D**54**, 905–921.
Cameron, J. S. & Simmonds, H. A. (1981). *J. Clin. Pathol.* **34**, 1245–1254.
Chenna, R., Sugawara, H., Koike, T., Lopez, R., Gibson, T. J., Higgins, D. G. & Thompson, J. D. (2003). *Nucleic Acids Res.* **31**, 3497–3500.
Collaborative Computational Project, Number 4 (1994). *Acta Cryst.* D**50**, 760–763.
Colloc'h, N., El Hajji, M., Bachet, B., L'Hermite, G., Schiltz, M., Prange, T., Castro, B. & Mornon, J. P. (1997). *Nature Struct. Biol.* **4**, 947–952.
Colloc'h, N., Gabison, L., Monard, G., Altarsha, M., Chiadmi, M., Marassio, G., Sopkova-de Oliveira Santos, J., El Hajji, M., Castro, B., Abraini, J. H. & Prangé, T. (2008). *Biophys. J.* doi:10.1529/biophysj.107.122184.
Colloc'h, N., Girard, E., Dhaussy, A. C., Kahn, R., Ascone, I., Mezouar, M. & Fourme, R. (2006). *Biochim. Biophys. Acta*, **1764**, 391–397.
French, S. & Wilson, K. (1978). *Acta Cryst.* A**34**, 517–525.
Gabison, L., Chiadmi, M., Colloc'h, N., Castro, B., El Hajji, M. & Prangé, T. (2006). *FEBS Lett.* **580**, 2087–2091.
Imhoff, R. D., Power, N. P., Borrok, M. J. & Tipton, P. A. (2003). *Biochemistry*, **42**, 4094–4100.
Jones, T. A., Zou, J.-Y., Cowan, S. W. & Kjeldgaard, M. (1991). *Acta Cryst.* A**47**, 110–119.
Kahn, K., Serfozo, P. & Tipton, P. A. (1997). *J. Am. Chem. Soc.* **119**, 5435–5442.
Kahn, K. & Tipton, P. A. (1997). *Biochemistry*, **36**, 4731–4738.
Kahn, K. & Tipton, P. A. (1998). *Biochemistry*, **37**, 11651–11659.
Laskowski, R. A., MacArthur, M. W., Moss, D. S. & Thornton, J. M. (1993). *J. Appl. Cryst.* **26**, 283–291.
Lovell, S. C., Davis, I. W., Arendall, W. B. III, de Bakker, P. I. W., Word, J. M., Prisant, M. G., Richardson, J. S. & Richardson, D. C. (2003). *Proteins*, **50**, 437–450.
Matthews, B. W. (1968). *J. Mol. Biol.* **33**, 491–497.
Navaza, J. (1994). *Acta Cryst.* A**50**, 157–163.
Otwinowski, Z. & Minor, W. (1997). *Methods Enzymol.* **276**, 307–326.
Pfleiderer, W. (1974). *Liebigs Ann. Chem.* **11**, 2030–2045.
Pflugrath, J. W. (1999). *Acta Cryst.* D**55**, 1718–1725.
Pui, C. H., Relling, M. V., Lascombes, F., Harrison, P. L., Struxiano, A., Mondesir, J. M., Ribeiro, R. C., Sandlund, J. T., Rivera, G. K., Evans, W. E. & Mahmoud, H. H. (1997). *Leukemia*, **11**, 1813–1816.
Ramachandran, G. N., Ramakrishnan, C. & Sasisekharan, V. (1963). *J. Mol. Biol.* **7**, 95–99.
Raychaudhuri, A. & Tipton, P. A. (2002). *Plant Physiol.* **130**, 2061–2068.
Retailleau, P., Colloc'h, N., Vivarès, D., Bonneté, F., Castro, B., El Hajji, M., Mornon, J.-P., Monard, G. & Prangé, T. (2004). *Acta Cryst.* D**60**, 453–462.
Retailleau, P., Colloc'h, N., Vivarès, D., Bonneté, F., Castro, B., El Hajji, M. & Prangé, T. (2005). *Acta Cryst.* D**61**, 218–229.
Rozenberg, S., Roche, B., Dorent, R., Koeger, A. C., Borget, C., Wrona, N. & Bourgeois, P. (1995). *Rev. Rhum. Engl. Ed.* **62**, 392–394.
Sarma, A. D., Serfozo, P., Kahn, K. & Tipton, P. A. (1999). *J. Biol. Chem.* **274**, 33863–33865.
Sayle, R. A. & Milner-White, E. J. (1995). *Trends Biochem. Sci.* **20**, 374–376.
Sevenian, A., Davies, K. J. & Hochstein, P. (1991). *Am. J. Clin. Nutr.* **54**, 1129–1134.
Terkeltaub, R. A. (1993). *Curr. Opin. Rheumatol.* **5**, 510–516.
Wu, X., Muzny, D. M., Lee, C. C. & Caskey, C. T. (1992). *J. Mol. Evol.* **34**, 78–84.